Methodological Bias between Trajectory Geometric Co-location and Air-Parcel Lagrangian Co-location: Evidence from UAV Re-penetration Observations over the Western Sichuan Plateau

Huijing Li[a]

[a] *Weather Modification Office of Sichuan Province, Chengdu 610072, China*

Corresponding author: Huijing Li, 942923956@qq.com

Peer review status:

This is a non-peer reviewed preprint submitted to EarthArXiv.

Methodological Bias between Trajectory Geometric Co-location and Air-Parcel Lagrangian Co-location: Evidence from UAV Re-penetration Observations over the Western Sichuan Plateau

Huijing Li[a]

[a] *Weather Modification Office of Sichuan Province, Chengdu 610072, China*

Corresponding author: Huijing Li, 942923956@qq.com

ABSTRACT

Whether "trajectory geometric co-location" is equivalent to "air-parcel Lagrangian co-location" remains a methodological blind spot in evaluating UAV cloud-seeding re-penetration (the UAV performed a repeated cloud penetration—hereafter, re-penetration—to re-sample the same cloud volume). Using silver iodide (AgI) seeding observations from a Wing Loong-2 UAV flight over the Western Sichuan Plateau on 15 February 2026, together with three-station soundings, ERA5 reanalysis, and airborne measurements, we quantify the bias between the two frameworks. At the ERA5 horizontal wind speed of 13.1 m s^{-1} at the seeding altitude (≈6.68 km), the plume advective displacement over 53 min is about 41.6 km, comparable to the 49.1 km longitudinal span of Window A; the geometrically co-located window therefore very likely no longer enclosed the same air mass (i.e., geometric co-location ≠ Lagrangian co-location). Three-dimensional geometric co-location yields a size spectrum ratio R(D) ≈ 1.0, which, given the available data, cannot be distinguished as either (i) persistence of the seeded plume or (ii) sampling of fresh upwind background air whose concentration happens to match that of the initial seeding leg. Lon-only co-location, by contrast, produces a spurious decay (R(D) = 0.67/0.60/0.58). We propose methodological protocols for re-penetration evaluation and operational recommendations for Lagrangian tracking (wind-offset flight tracks, dual-aircraft coordination, inert tracers, and FLEXPART-type dispersion modeling), and stress that, because Leg1 is itself a seeding leg with no unseeded baseline, re-penetration evaluations must state this limitation explicitly. The results provide a quantitative basis for the methodological design of UAV seeding-effect verification over the plateau.

Keywords: geometric co-location; Lagrangian co-location; UAV observations; Western Sichuan Plateau

1. Introduction

a. Research background and significance

The core difficulty in evaluating the effect of cloud seeding for rain (or snow) enhancement lies in reliably attributing observed cloud microphysical changes to the seeding operation rather than to the natural evolution of the cloud system. This attribution problem is, in essence, a methodological one: without an effective means of extracting a "response signal," any effect conclusion lacks firm observational support.

Among current approaches to effect verification, the 're-penetration' strategy is widely regarded as offering a distinct advantage: after the seeding operation, the aircraft returns to the previously sampled airspace and samples again, using the change in microphysical state at the same spatial location as a potential response signal. In principle, this method removes much of the noise introduced by cloud-system displacement and macroscale evolution, and it has therefore received increasing attention in recent aircraft seeding observation campaigns and is regarded as a frontier path for effect evaluation (Wang et al. 2013; Wang et al. 2017).

However, a fundamental prerequisite has long been overlooked: what does 'the same location' physically mean? In existing re-penetration observations, 'co-location' is vaguely understood as the mere spatial overlap of flight tracks in longitude and latitude. Yet upper-level winds persist; the seeded air parcel may have been advected tens of kilometers by the background wind during the time interval between the two passes. Under such conditions, the "same location" within a fixed longitude–latitude grid may in fact correspond to entirely different air parcels. This problem is particularly acute over the Western Sichuan Plateau, where upper-level winds are persistently strong in winter. Without proper distinction, the "air replacement" caused by advection could be misread as either "in situ persistence" or "in situ decay" of the seeded plume, seriously compromising the reliability of the evaluation. We address precisely this long-overlooked prerequisite and establish a more rigorous physical basis for re-penetration observations.

b. Domestic and international practices and the present methodological classification

In domestic and international aircraft seeding observation campaigns, "re-penetration" has been adopted repeatedly as an operational design. For example, in the aircraft rain-enhancement trials over the Sanjiangyuan region, "zigzag seeding operations with re-penetration sounding" were conducted (Wang et al. 2013), analyzing microphysical response by comparing changes in liquid cloud particles and ice crystal concentrations before and after seeding. In the international literature, aircraft observations for cloud-seeding verification commonly emphasize repeated sampling along similar tracks before and after operations to obtain time series of cloud microphysical parameters (Li et al. 2022).

Nevertheless, the above practices share a common methodological blind spot: although they achieve "overlap in flight-track space," they never rigorously establish which physical framework that overlap actually represents. In other words, "co-location" has long been treated as a self-evident operational concept, lacking a precise methodological definition and classification.

We propose and rigorously distinguish, at the methodological level, between two fundamentally different co-location framings:

(1) *Trajectory geometric co-location*: an Eulerian fixed-spatial-coordinate framework that uses the geometric overlap in longitude–latitude (and altitude) as the criterion for defining the 'same airspace.' This is the default operational framing adopted by the vast majority of re-penetration observations (Axisa and DeFelice 2016).

(2) *Air-parcel Lagrangian co-location*: a Lagrangian framework that retrieves the air-parcel trajectory along the ambient wind field so that the two sampling passes before and after seeding correspond to physically "the same seeded air parcel" (Axisa and DeFelice 2016). This framing is the most physically rigorous, yet it has almost never been systematically implemented or quantitatively evaluated in operational UAV re-penetration practice.

Building on this dichotomy, we synthesize the implicit co-location criteria found in existing re-penetration literature into three levels of increasing physical rigor: (a) lon-only co-location, which ignores latitude and altitude differences, is the most prone to sample confusion; (b) three-dimensional (3D) spatial co-location adds an altitude constraint on top of longitude and latitude but remains within the Eulerian framework; (c) Lagrangian co-location tracks the same air parcel and is the most physically rigorous. This three-level classification is not a restatement of existing summaries but an analytical framework proposed in our study to diagnose co-location bias.

c. Research gaps and our study's objectives

Under the above original classification framework, the following three methodological questions have never been systematically addressed with observational data:

(1) Under realistic plateau strong-advection conditions, how large is the spatial bias between "geometric co-location" and "Lagrangian co-location," and what physical factors determine its magnitude?

(2) For the same set of before- and after-seeding observation samples, do the size spectrum ratios obtained under geometric co-location (lon-only or 3D) and under Lagrangian co-location differ systematically? If so, which framing better reflects the true physical process?

(3) How should the longitude, latitude, altitude, and time tolerances of the co-location window be set according to the physical scale of advective displacement, so that "co-location" holds simultaneously in both statistical and physical senses?

The central objective of our study is to use the Wing Loong-2 UAV re-penetration observations over the Western Sichuan Plateau on 15 February 2026, together with soundings from three stations and the ERA5 reanalysis wind field, to quantify the bias between geometric co-location and Lagrangian co-location; to reveal how the choice of co-location framing directionally affects the size-spectrum-ratio conclusion; and, on that basis, to propose co-location window-setting criteria and operational recommendations suited to the strong-advection conditions of the plateau.

We make three methodological contributions. First, we are the first to propose and define the dichotomy of trajectory geometric versus air-parcel Lagrangian co-location and to build a three-level framework for co-location framings. Second, using observed wind fields, we quantify the spatial bias between the two framings and demonstrate that geometric co-location ≠ Lagrangian co-location. Third, we offer window-design criteria anchored on advective displacement, thereby providing an operational protocol for future UAV re-penetration verification over the plateau.

2. Data and Methods

a. Flight observation and seeding operation overview

On 15 February 2026, the Wing Loong-2 UAV flew from 1400 to 2037 Beijing Time (hereafter BJT) and seeded from 1608 to 1906 BJT. Twenty cold-cloud smoke flares were deployed, and the cumulative dose increased monotonically with time. The flight adopted a typical lawnmower pattern (Fig. 1): Leg1 seeded continuously from east to west (101.5°→99.6°E), followed by four north–south short transects (Leg2/3/4/5) repeatedly swept across the target, and Leg6 flew east for recovery. Legs 1–5 were all within the seeding phase.

Leg3 and Leg5 re-penetrated the 99.6–100.1°E and 100.3–100.7°E longitude bands, respectively, that Leg1 had seeded earlier, representing repeated sampling of the same seeding region under different accumulated-dose-and-time conditions.

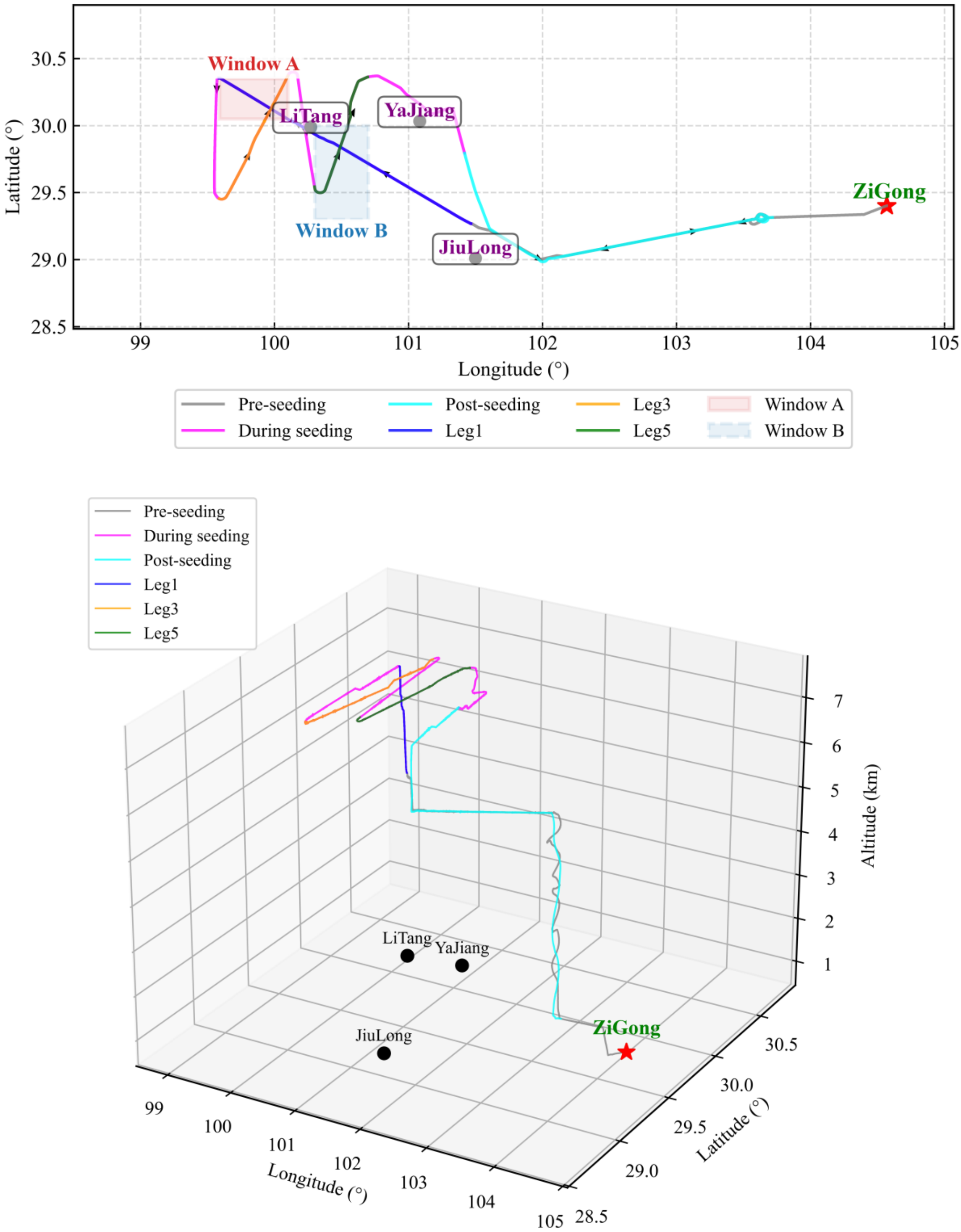

Fig. 1. Flight track of the Wing Loong-2 UAV on 15 February 2026: (a) horizontal projection and (b) altitude–longitude–latitude view. In both panels the gray, magenta, and cyan lines denote the pre-seeding, during-seeding, and post-seeding phases of the flight,

respectively, while the dark blue, orange, and green lines mark Leg1, Leg3, and Leg5. The shaded rectangles mark Window A and Window B analyzed in section 2c. Gray dots mark the geographic reference points Litang, Yajiang, and Jiulong, and the red star marks the launch site at Zigong.

b. Data and quality control of the observations

We use sounding data from the Ganzi (elevation 3379 m), Batang (2581 m), and Jiulong (2920 m) stations on the flight day, together with ECMWF ERA5 3-hourly reanalysis data (horizontal resolution 0.25° × 0.25°). The ERA5 data were converted to BJT and aligned with the observation period; the study domain is 99.0°–101.5°E, 29.5°–30.8°N.

The Wing Loong-2 UAV was equipped with three probes of the NORINCO (China North Industries Group) UAV sounding system, configured as follows: Cloud (CDP, 2–50 μm, 32 channels); CloudPic (CIP, 25–1550 μm, 62 channels, 25 μm step); and RainPic (PIP, 100–6200 μm, 62 channels, 100 μm step) (Korolev et al. 2014). Auxiliary data include GPS longitude, latitude, and altitude, pressure altitude, ambient temperature, sampling airspeed, and true airspeed.

The observation data underwent rigorous quality control. When the number concentration exceeded 500 cm^{-3}, a coincidence correction was applied to the CDP, with correction probability

$$P = 1 - e^{-\lambda\tau} \quad (1)$$

where

$$\lambda = N \cdot SA \cdot TAS \quad (2)$$

with SA = 0.336 mm^2, N the particle number concentration, and TAS the sampling airspeed.

CIP and PIP rejected shattered particles based on the inter-arrival time threshold, set to CIP $\leq 2\times10^{-5}$ s and PIP $\leq 1\times10^{-4}$ s; particles shorter than the threshold, together with their preceding particle, were assigned a zero count (Korolev and Isaac 2005). Stuck (failed) diodes (trigger frequency deviating from the median by >3σ), streak particles (aspect ratio >5 and width ≤2 pixels), and the first channel (CIP 25 μm, PIP 100 μm) were all removed, with the removed channels supplemented by CDP and CIP. CIP/PIP data were processed with standard image-level quality control (shatter rejection, stuck-diode removal, streak-particle removal, first-channel removal).

For quality control of derived quantities, spike detection used a dual criterion of median-filter residual >5 times the robust standard deviation and duration not exceeding 2 s, flagging as suspect without hard truncation, so as to avoid deleting genuine extreme cloud structures. Liquid water content (LWC) exceeding 5 g m^{-3} was flagged, and such extreme values were subjected to focused re-examination.

Spectral processing used the per-channel sampling-volume method to avoid underestimation of the large-particle end inherent in a uniform volume (Korolev et al. 2014). The depth of field

$$DOF_i = \frac{c \cdot D_i^2}{(4\lambda)}, c = 6 \quad (3)$$

with λ = 0.658 μm the laser wavelength; the effective array width

$$EAW_i = (N_{diode} - 1) \cdot d_{res} - D_i \quad (4)$$

(where N_diode = 64 is the number of diodes and d_res is the channel resolution). The sampling volume of the *i*-th size channel is

$$SV_i = TAS \cdot \Delta t \cdot DOF_i \cdot EAW_i \quad (5)$$

Here TAS is the instrument sampling airspeed per channel; erroneously using true airspeed would introduce a systematic bias of about 15% in dN/dD. The per-channel size spectrum is

$$\frac{dN}{dD} = \frac{count_i}{(SV_i \cdot \Delta D_i)} \quad (6)$$

where count_i is the particle count in the channel and ΔD_i is the channel width. CDP (2–50 μm), CIP (25 μm–1 mm, first channel removed), and PIP (1–6.2 mm) were concatenated, with the overlap region taken from CDP.

We use the 5th–95th percentile band to characterize uncertainty: for all valid 1-Hz records within a window, the 5th and 95th percentiles of each size channel are computed along the record axis; the shaded band is the range encompassing the middle 90% of samples. This statistic is insensitive to skewness and extremes and more robustly depicts the natural variability of dN/dD. The figures additionally overlay 200 randomly sampled single-pass scatter points to illustrate the spatiotemporal fluctuation of particle concentration. Note that this shaded band represents the middle 90% range of the sample (i.e., the natural dispersion of single passes), not a statistical confidence interval, and should not be used for significance inference.

c. Re-penetration co-location analysis method

To judge whether the two-pass observations targeted the same air parcel, we define a number-concentration size-ratio index

$$R(D) = \frac{N_{repen}(D)}{N_{seed}(D)} \tag{7}$$

where N_seed(D) and N_repen(D) denote the number concentration density in the same size channel of the initial seeding leg (Leg1) and the re-penetration leg, respectively (computed by the per-channel sampling-volume method of section 2b). If R(D) ≈ 1, the particle concentration at that size bin shows no marked change between the two detections. Because Leg1 itself is a seeding leg rather than an undisturbed background cloud, R(D) is not interpreted as a "seeding effect" but only as a descriptive index of "whether the physical state of this air mass was stable between the two passes." The uncertainty of each channel is given by the bootstrap (2000 resamples) 95% confidence interval (Efron and Tibshirani 1993; Davison and Hinkley 1997).

The co-location window is not simply a drawn longitude range; both passes must fall within the same longitude–latitude region to qualify as repeated observation of the same air mass. Following this principle, we examined the overlap of Leg1 with each re-penetration leg in turn and selected two 3D co-location windows. Figure 2 plots the several re-penetrations in a longitude–latitude–time frame and is colored by the 75-μm channel (the small-ice-particle channel with the highest detection rate and most continuous spatial coverage) to illustrate the spatial positions of Window A and Window B. Window A (blue box) lies in the rectangle [99.59°–100.10°E, 30.05°–30.35°N]; Leg3 re-penetrated at nearly the same longitude and latitude about 53 min later, satisfying the 3D co-location with both longitude and latitude constraints and with sufficient sample size for direct quantitative analysis. Window B (red box) lies in the longitude band 100.3°–100.7°E; Fig. 2a shows both Leg1 and Leg5 cloud penetrations fall into the same longitude band, and their latitudes overlap in [29.72°–29.94°N], but the diagnosis shows that within the overlap band Leg5 contained particles in only 13.2% of rows, with a mean count of 14.3 per row, whereas outside the band at other latitudes 54.8% of rows contained particles with a mean count of 105.6 per row. The vast majority of Leg5 cloud particles lie at other latitudes outside the overlap band; restricting to the 3D-co-located portion would discard almost all of Leg5's cloud, and the resulting ratio would no longer reflect cloud change. Therefore Window B is treated only as lon-only co-location, not as a quantitative 3D co-location, and serves solely as a longitudinal contrast and methodological illustration.

The figure also shows that the 75-μm concentration of the seeding legs remained relatively high, providing the spatial background for the subsequent co-location ratio analysis. Geometric co-location is not equivalent to Lagrangian co-location; when the same location is passed twice, the air parcel may have long since been replaced.

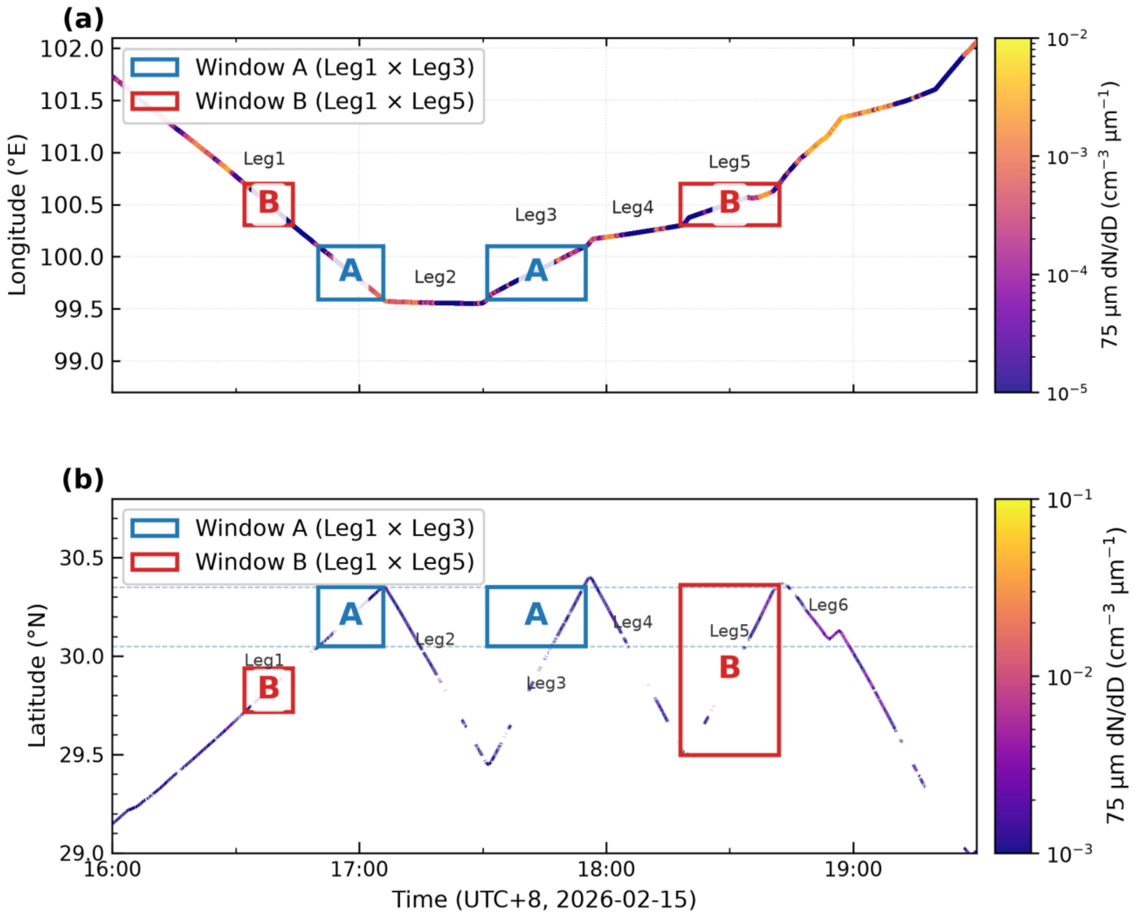

Fig. 2. Longitude–time (a) and latitude–time (b) distributions of the flight track. Color denotes dN/dD of 75-μm particles. Blue box = Window A (Leg1 ∩ Leg3, 99.59–100.10°E); red box = Window B (Leg1 ∩ Leg5, 100.3–100.7°E).

Leg4 is a turning segment with a short track and very few sampling points, lacking an effective sample size for statistical comparison with Leg1, and is therefore excluded from the co-location analysis.

Furthermore, the above co-location refers to the geometric overlap of tracks within an Eulerian fixed-spatial window (synchronized sampling based on spatial coordinates), not Lagrangian-type co-location that follows the motion of the seeded air parcel; under a pronounced horizontal wind the two are not equivalent (see the quantitative argument in section 4a).

d. Multi-source cross-validation and vertical diagnosis method

The two types of data are independent and constrain each other hierarchically: soundings provide stratification and wind profiles, ERA5 provides circulation. Cross-validation (Table 1) includes: (1) the ambient temperature at the seeding altitude (6680 m) compared among airborne, sounding-interpolated, and ERA5-interpolated values; (2) in-cloud wind speed and direction compared between sounding and ERA5 interpolation.

Vertical misalignment diagnosis: taking the ERA5 maximum-cloud-water-content layer as the "supercooled-water-rich layer," its height difference from the seeding altitude is Δh; we also derive the altitude range corresponding to the AgI high-efficiency nucleation window (−8 to −15°C) and compare it with the seeding altitude to judge whether the latter falls within the 'can-nucleate-and-can-grow' range. The plume advective displacement $L = |V| \cdot \Delta t$ is estimated from the ERA5 wind speed at the seeding altitude and the re-penetration time difference, and compared with the longitudinal span of the co-location window to assess the validity of Lagrangian co-location.

Table 1. Cross-validation of key diagnostic quantities among multiple data sources.

Diagnostic	**Airborne in situ**	**Sounding**	**ERA5**	**Consistency**
6680-m temperature (°C)	−23 to −25	−23.1 (Ganzi 2000 BJT)	−23.1	Excellent
Horizontal wind at seeding altitude	—	10–20 $m\ s^{-1}$, westerly (four sounding times)	13.1–16.0 $m\ s^{-1}$, westerly	Excellent

Consistency is rated as follows: Excellent = numerical difference within observational uncertainty; Good = consistent magnitude and structure with small numerical deviation; Fair = consistent structure but significant absolute discrepancy.

3. Co-location Comparison Results and Methodological Tests

a. Window A: size spectrum ratio under 3D geometric co-location

The strict 3D co-location comparison for Window A (Figs. 3, 4; Table 2) shows that the size spectrum ratio of Leg3 relative to Leg1 is R(D) = 1.05 at 75 μm, 0.93 at 250 μm, 1.17 at 600 μm, and 0.96 averaged over 25–200 μm; the confidence intervals of all four indicators span 1.0. Combined with the key-size time series (Fig. 3), the dN/dD of the 75-, 250-, and 600-μm channels along Leg3 remained near the Leg1 magnitude throughout, without systematic enhancement or decay. This indicates that the number-concentration size distributions in the Leg3 re-penetration window and the Leg1 initial seeding leg are essentially unchanged.

Table 2. Three-dimensionally co-located size spectrum comparison for Window A (Leg1 vs Leg3) on 15 February 2026.

Diameter D (μm)	**Strict 3D ratio R(D)**	**bootstrap 95% CI**	**lon-only ratio**	**Leg1 sample size (with particles)**	**Leg3 sample size (with particles)**
75	1.05	[0.90, 1.22]	0.67	927 (790)	462 (446)
250	0.93	[0.79, 1.09]	0.60	927 (790)	462 (446)
600	1.17	[0.86, 1.57]	0.58	927 (790)	462 (446)
25–200 (mean)	0.96	[0.83, 1.11]	0.61	927 (790)	462 (446)

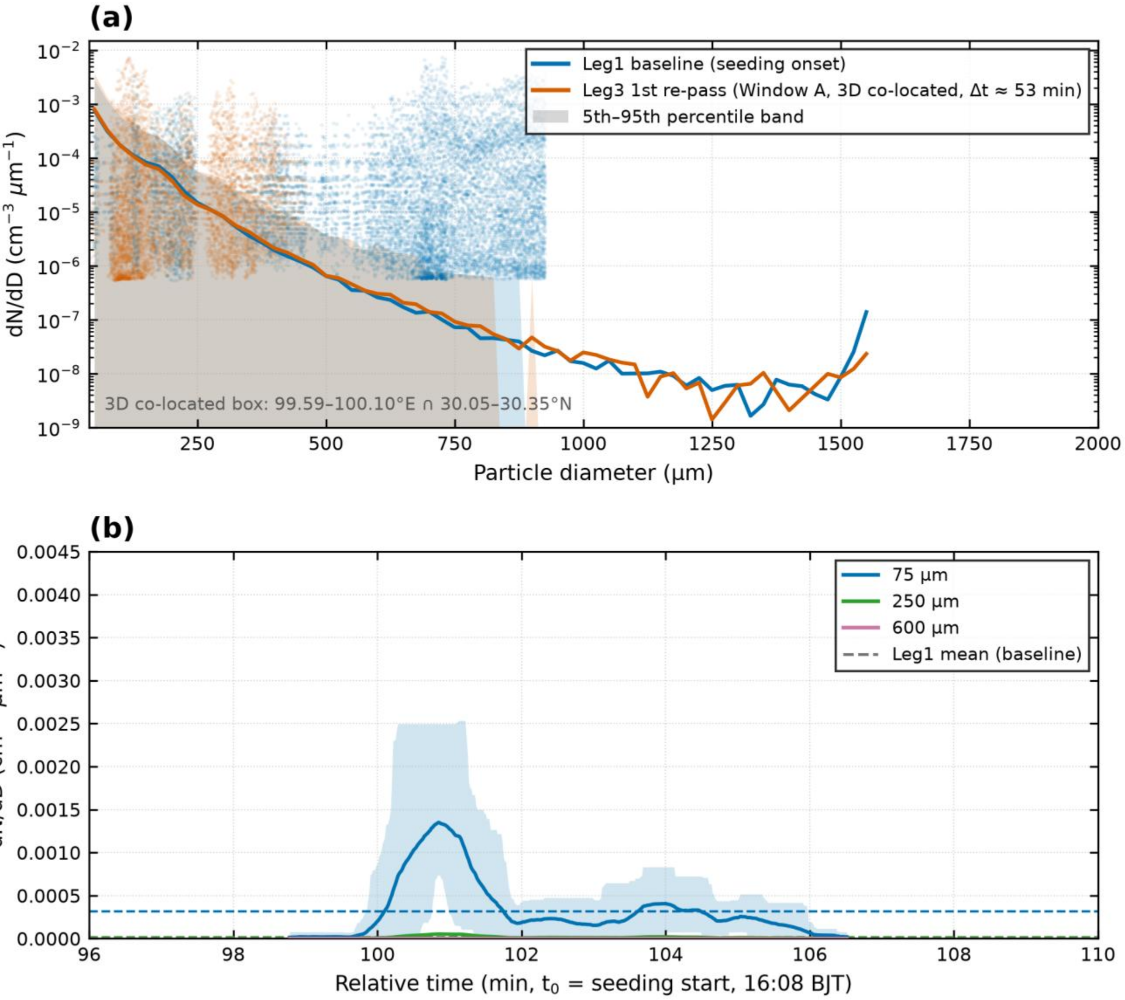

Fig. 3. Size spectrum comparison (a) and temporal evolution of dN/dD at 75, 250, and 600 µm along Leg3 (b) under 3D co-location for Window A of the AgI-seeded terrain cloud over the Western Sichuan Plateau on 15 February 2026. Shaded bands denote the 5th–95th percentile range; faint dots are 200 per-leg sampled single passes; colored dashed lines mark the Leg1 baseline.

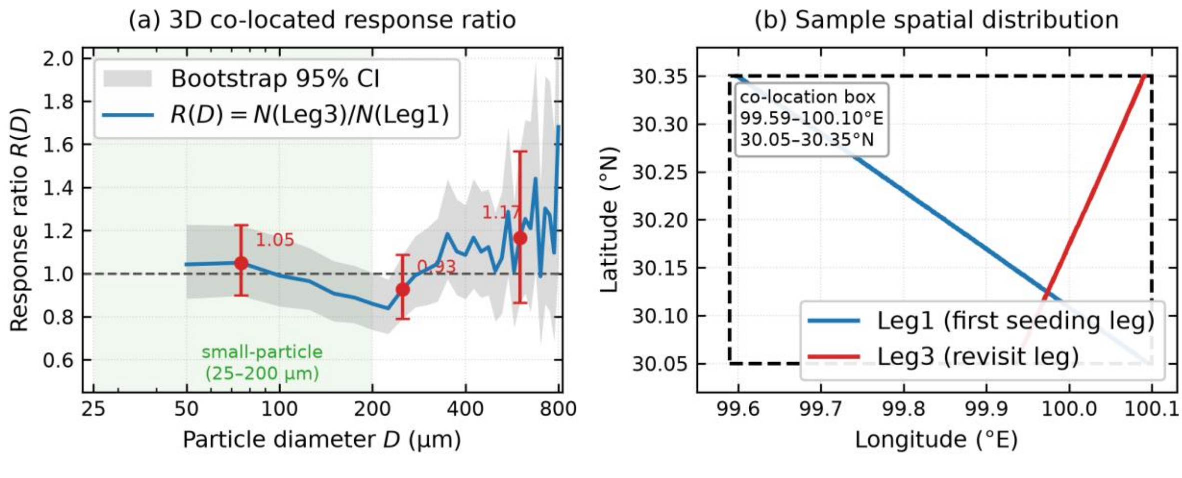

Fig. 4. Three-dimensionally co-located size spectrum ratio for Window A (Leg1 vs Leg3). (a) Co-located response ratio R(D) versus particle diameter (log axis); dashed line is the R = 1.0 baseline; red markers indicate ratios at 75/250/600 µm (error bars: bootstrap 95%

CI). (b) Spatial distribution of Leg1 (blue) and Leg3 (red) samples; the black dashed rectangle denotes the overlap box 99.59–100.10°E × 30.05–30.35°N.

Because Leg1 itself is a west-flying seeding leg and not unseeded, R(D) ≈ 1 means that the particle concentration in the re-penetration window about 53 min after the first seeding is comparable to that of the initial seeding leg. This admits two interpretations: (1) the plume/ice crystals produced by seeding persisted in this region, with concentration not diluted by diffusion; (2) the plume had moved out of the window with the westerly wind, and what Leg3 sampled was fresh upwind air whose natural background concentration happened to be close to that of the Leg1 seeding leg. Because this case is a single-aircraft, single-flight observation lacking both an unseeded baseline and Lagrangian trajectory tracking, the available data cannot distinguish which situation applies (quantitative argument in section 4a). Therefore we can only describe the result as "the re-penetration window concentration is comparable to that of the initial seeding leg," and cannot prove "plume persistence" or "post-seeding concentration maintenance."

The methodological contrast is clear: if one uses only lon-only co-location and drops the latitude constraint, the ratio for the same pair of legs (Table 2) shows an apparent 'decay.' This decay is an artifact of latitudinal misalignment: Leg1 and Leg3 sampled different latitude distributions within the same longitude band, producing an apparent difference through mixing of particles from different latitudes. This contrast directly illustrates the decisive influence of co-location window selection on the conclusion. Hence, in selecting the co-location window, we strictly adhere to 3D co-location, choosing Window A as the quantitative research object, while Window B serves only as a methodological contrast (see section 2c).

Under 3D geometric co-location, the ratios of channels larger than 800 μm cannot be computed (most samples below detection limit), and this size range is excluded from the co-location ratio analysis. Although the 600-μm ratio of 1.17 is slightly greater than 1, its confidence interval [0.86, 1.57] is wide and spans 1.0, insufficient to support a judgment of "significant increase in large particles."

Window A adopts the strict 3D co-location with both longitude and latitude constraints and is the only quantitative co-location window in our study. Figure 3a shows that the size spectra of Leg3 (re-penetration about 53 min after seeding) and Leg1 (initial seeding leg) almost coincide in the 25–200 μm range, with very low number concentrations at the large-particle end (>400 μm). In Fig. 3b the dN/dD of each Leg3 channel always falls within the 5th–95th percentile band near the Leg1 baseline.

Both Leg1 and Leg3 are seeding legs (seeded = 1); the result therefore characterizes only the re-penetration-window concentration relative to the initial seeding leg and cannot be used to infer plume growth or decay (sections 4a, 4c).

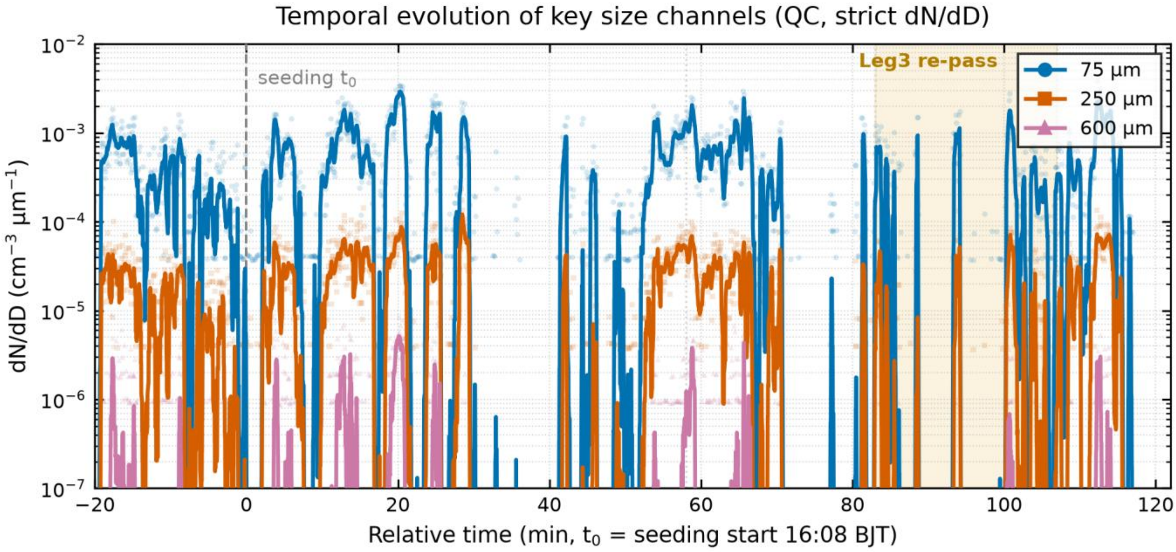

Fig. 5. Temporal evolution of number concentration density dN/dD at key size channels (strict method, QC data). dN/dD at 75/250/600 μm versus relative time (t_0 = seeding start 1608 BJT); gray dashed line marks the seeding start, orange shaded band marks the Leg3 re-penetration window (17:31–17:55 BJT, ≈+83–+107 min after seeding start; ~53 min after the mean Leg1 sampling in Window A). Thin dots are individual samples, thick line is the moving average.

Figure 5 corroborates the comparable-concentration result for Window A from a time-series perspective. During the Leg3 re-penetration window (about 53 min after the initial Leg1 sampling), the dN/dD of all three channels fell back and stabilized at the Leg1 baseline magnitude (R(D) ≈ 1.0), with no obvious concentration growth or decay trend.

b. Window B: contrast ratio under lon-only co-location

Window B corresponds to the Leg5-versus-Leg1 comparison (Fig. 6), with a time interval of 110 min and a longitude overlap band of 100.3–100.7°E. Leg1 is the initial seeding leg of that longitude band, and Leg5 is the re-penetration leg about 70–120 min later. We treat Window B only as a longitudinal contrast and methodological illustration, and do not adopt any maintenance or decay magnitude derived therefrom as a physical conclusion.

To complete the methodological contrast, we also computed the lon-only co-location ratio for Window B (Leg5/Leg1): 75 μm = 0.91, 250 μm = 0.75, 600 μm = 1.23. Although this window cannot satisfy 3D co-location, it yields one qualitative conclusion: about 110 min after the Leg1 passage in this longitude band, the spatial distribution of particle concentration within this longitude band had clearly changed from that at the initial seeding moment, indicating spatial reorganization of the plume field. Combined with the wind-field analysis in section 4a, this reorganization should be a natural process of advective transport rather than the dissipation of the silver iodide plume.

Care is needed with the 'lon-only' terminology: the lon-only construct used here (Window B, Leg5/Leg1, ratios 0.91/0.75/1.23) and the latitude-constraint-lifted Window A lon-only of section 3a (ratios 0.67/0.60/0.58) are both labeled lon-only but are constructed differently: the former is a real comparison of two different legs (Leg5 re-penetration and Leg1 first seeding) under longitude-only overlap, used to qualitatively show plume spatial reorganization; the latter is a spurious decay obtained by artificially removing the latitude constraint from the same Window A, used to illustrate the decisive influence of the latitude constraint on the co-location conclusion. The two must not be confused.

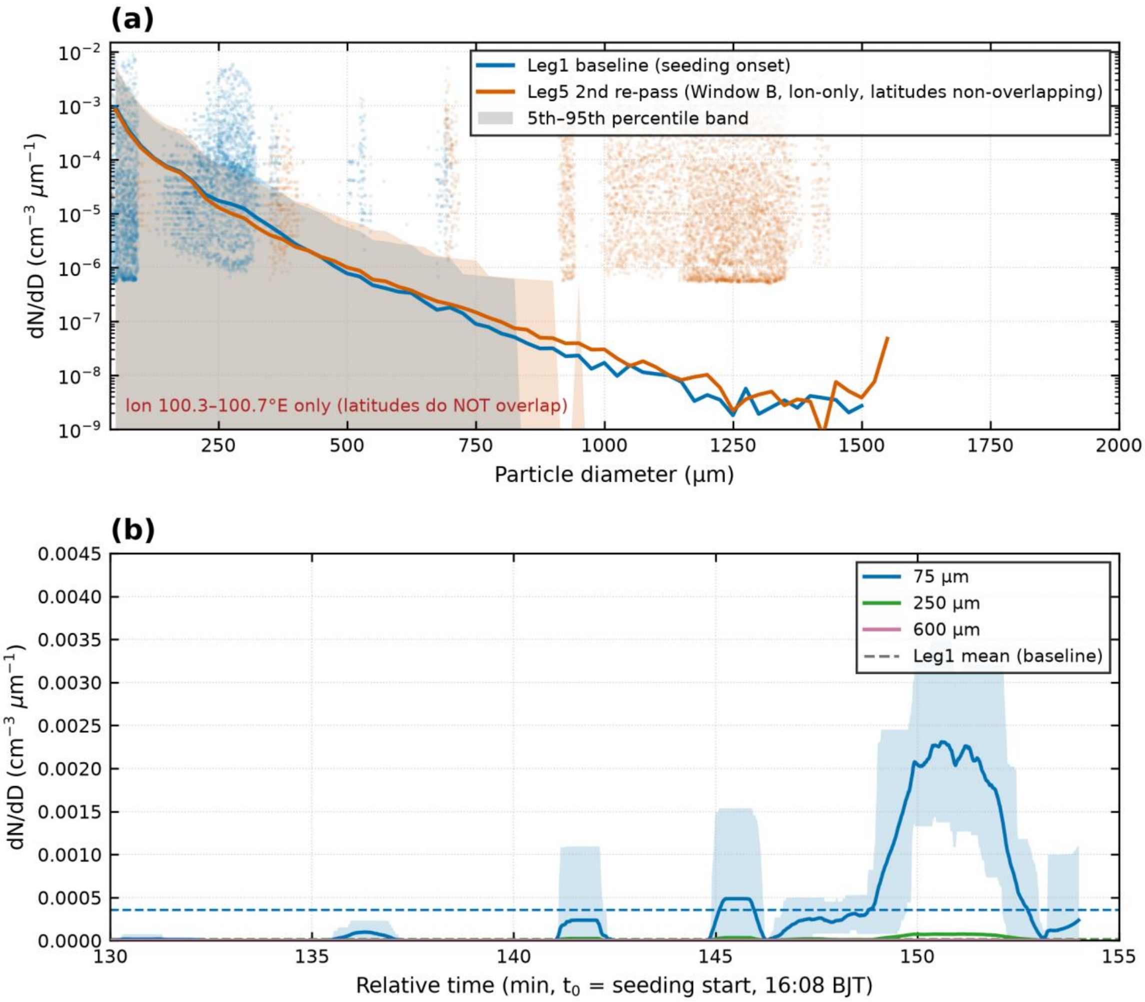

Fig. 6. Lon-only window (100.3–100.7°E) size spectrum comparison for Window B (Leg1 vs Leg5) (a) and Leg5 evolution (b).

4. Discussion

a. Methodological reflection on geometric versus Lagrangian co-location

The central methodological proposition of our study is: trajectory geometric co-location (comparing before- and after-concentration within a fixed longitude–latitude rectangle) is not equivalent to air-parcel Lagrangian co-location (following the same seeded air parcel). Under a pronounced horizontal wind, the two exhibit a systematic spatial bias, yet previous re-penetration evaluations often made no such distinction.

This case permits a quantitative assessment of the problem. The wind speed at the seeding altitude was 13.1 m s^{-1} according to ERA5 (10–20 m s^{-1} from the three-station soundings), predominantly westerly. Accordingly, the plume advective displacement over 53 min is about 41.6 km, or 0.43° longitude; over 110 min about 86.4 km, or 0.90° longitude. Window A's longitudinal span is 99.59–100.10°E, i.e., 0.51° or 49.1 km. The two are of the same order of magnitude, meaning that after 53 min the air originally inside Window A had moved noticeably eastward with advection, and the geometrically co-located window very likely no longer enclosed the same air mass; if the plume moved east with the westerly, the plume within the original window had shifted to about 100.02–100.53°E, while Leg3, sampling at 99.6–100.1°E, intercepted the fresh upwind air flowing in from upstream (to the west).

Thus the R(D) ≈ 1.0 result admits two interpretations that the available data cannot distinguish (section 3a). The more critical limitation is that Leg1 itself is a seeding leg with no unseeded baseline; even with perfect Lagrangian co-location, the Leg1–Leg3 comparison cannot separate natural background from seeding increment. The conclusion is therefore stated as comparability, not persistence.

To truly achieve Lagrangian tracking, subsequent observations need to satisfy at least one of the following: (1) design the re-penetration track to drift downstream following the real-time wind field, rather than repeatedly sweeping a fixed longitude band; (2) employ dual- or multi-aircraft coordination, with one aircraft at the seeding point and one at the predetermined downstream drift position sampling synchronously; (3) incorporate an inert tracer (e.g., SF_6 or an identifiable chemical tracer) to confirm that the sampled air is indeed the seeded parcel; (4) use mesoscale-model Lagrangian particle dispersion simulation (e.g., FLEXPART-type) to forecast plume position and adjust the track accordingly. These constitute the most operationally valuable methodological recommendations of our study.

Based on a single flight, we offer a quantitative caveat: the bias between trajectory geometric co-location and air-parcel Lagrangian co-location is a kinematic necessity, and a single case already reveals this systematic problem; multi-case statistics are a next step and do not affect the validity of the directional conclusions of our study.

b. Application recommendations for rain-enhancement observations

Based on the diagnosis of our study, we offer methodological recommendations for observation design: shift the observation strategy to a Lagrangian design, in which the re-penetration leg is offset downstream according to the real-time wind field, with the offset estimated as $L = |V| \cdot \Delta t$ (here 13.1 m s^{-1} × 53 min ≈ 42 km), so that the same seeded air parcel is observed; where conditions permit, adopt dual-aircraft coordination or add a tracer (see section 4a).

c. Uncertainty and limitations

Because of these limitations, the conclusions are framed only at the level the data support.

1. Spatiotemporal representativeness of reanalysis data: ERA5 has a horizontal resolution of 0.25° and a 3-h time interval; its vertical velocity is a grid-averaged value that systematically underestimates local in-cloud updrafts. We use it as a lower bound.

2. Fundamental limitation of the co-location framing: geometric co-location is not equivalent to Lagrangian co-location, and the two interpretations of $R(D) \approx 1.0$ cannot be distinguished with the available data. This is the most important methodological limitation of our study.

3. Spatiotemporal representativeness of soundings: the three-station soundings cover only the 0800 and 2000 BJT times; the operation period (1600–1900 BJT) has no synchronous sounding, and the 2000 BJT sounding actually reflects the stratification from the late operation through after its end; the three stations are all tens of kilometers or more from the operation center. We partially compensate for this deficiency through cross-validation of the three-station consistency with ERA5 and airborne measurements.

5. Conclusions

We draw the following conclusions:

1. It is quantitatively confirmed that trajectory geometric co-location ≠ air-parcel Lagrangian co-location: under a horizontal wind of 13.1 m s^{-1} at the seeding altitude, the 53-

min advective displacement is about 41.6 km, of the same order as the 49.1-km longitudinal span of Window A; the geometrically co-located window no longer enclosed the same air mass at re-penetration.

2. The 3D co-location size spectrum ratio for Window A is R(D) = 1.05/0.93/1.17/0.96 (0.96 averaged over 25–200 μm), and all bootstrap 95% confidence intervals span 1.0; under either interpretation this result cannot distinguish between "plume persistence" and fresh upwind background air of comparable concentration.

3. The co-location framing determines the direction of the conclusion: 3D co-location gives $R \approx 1.0$, whereas lon-only co-location gives a spurious decay R = 0.67/0.60/0.58, highlighting the decisive influence of window selection on re-penetration evaluation.

4. Methodological recommendation: the re-penetration track should be offset downstream by $L = |V| \cdot \Delta t$, should adopt dual-aircraft coordination or a tracer, and should be supplemented by Lagrangian particle dispersion simulation, so as to achieve true air-parcel co-location.

In summary, re-penetration–co-location evaluation must shift from "geometric overlap of a fixed spatial window" to "Lagrangian tracking that follows the seeded air parcel"; otherwise the resulting "persistence/decay" conclusions are physically unreliable.

Acknowledgments.

The authors thank the Operations Monitoring Division of the Weather Modification Office of Sichuan Province for designing the seeding flight plan, the UAV operation team for conducting the UAV seeding and observation missions, and the staff of the Jiulong (56462), Batang (56247), and Ganzi (56146) upper-air sounding stations for providing the rawinsonde observations.

This research was supported by the Huayun Meteorological Technology Group Key Scientific Research Project (Grant JT-YF-202602).

Data Availability Statement.

The observational data used in our study are not publicly available due to operational restrictions. ERA5 reanalysis data are available from the Copernicus Climate Change Service. Radiosonde data are available from the China Meteorological Administration upon request.

REFERENCES

Axisa, D., and T. P. DeFelice, 2016: Modern and prospective technologies for weather modification activities: Developing a framework for integrating autonomous unmanned aircraft systems. Atmos. Res., 193, 1–12.

Davison, A. C., and D. V. Hinkley, 1997: Bootstrap Methods and Their Application. Cambridge University Press, Cambridge, 582 pp.

Efron, B., and R. J. Tibshirani, 1993: An Introduction to the Bootstrap. Chapman & Hall, New York, 436 pp.

Korolev, A., and G. A. Isaac, 2005: Shattering during sampling by OAPs and HVPS. Part I: Snow particles. J. Atmos. Oceanic Technol., 22, 528–542.

Korolev, A., C. Emersic, and R. Cresswell, 2014: A review of past and present developments of the forward scattering spectrometer probe. J. Atmos. Oceanic Technol., 31, 175–191, https://doi.org/10.1175/JTECH-D-13-00032.1.

Li, D., C. Zhao, Z. Yue, C. Liu, Y. Sun, and J. B. Cohen, 2022: Response of cloud and precipitation properties to seeding at a supercooled cloud-top layer. Earth Space Sci., 9, e2021EA001791, https://doi.org/10.1029/2021EA001791.

Wang, L., Y. Yin, Z. Yao, and A. Sun, 2013: Microphysical responses as seen in a stratocumulus aircraft seeding experiment in autumn over the Sanjiangyuan National Nature Reserve. Acta Meteor. Sinica, 71(5), 925–939, doi:10.11676/qxxb2013.070. [in Chinese]

Wang, Y., S. Niu, and H. Lei, 2017: An examination of the microphysical responses to aircraft seeding of stratiform clouds with embedded convection using the joint observational data of three aircraft. Trans. Atmos. Sci., 40(5), 686–696, doi:10.13878/j.cnki.dqkxxb.20161012002. [in Chinese]